ELSEVIER

Microporous and Mesoporous Materials 37 (2000) 233–242

MICROPOROUS AND MESOPOROUS MATERIALS

www.elsevier.nl/locate/micromeso

Cd-exchanged heulandite: symmetry lowering and site preference

Jano Stolz [a], Ping Yang [b], Thomas Armbruster [a,*]

[a] *Laboratorium für chemische und mineralogische Kristallographie, Universität Bern, Freiestrasse 3, CH-3012 Bern, Switzerland*
[b] *Shandong Institute of Building Materials, Applied Chemistry Department, P.O. Box 250022, Jinan, Shandong, People's Republic of China*

Received 21 July 1999; received in revised form 22 October 1999; accepted for publication 25 October 1999

Abstract

Fully Cd-exchanged heulandite was obtained from a Na-exchanged sample by treatment with 1 M Cd acetate solution at 373 K. Subsequent electron microprobe analyses revealed 4.0 Cd^{2+} per formula unit (pfu), that was in good agreement with 4.11 Cd pfu refined from single-crystal X-ray data collected at 293 K. Crystal structure refinements were performed in the space groups *C*2/*m*, *C*2, *Cm*, *C*$\bar{1}$, and *C*1, of which only the *Cm* model yielded reasonable agreement with the observed diffraction data. Cadmium preferentially occupied the center of the A channel, where it formed a distorted octahedral $Cd^{2+}(H_2O)_6$ complex, and a central position in the B channel that was sevenfold coordinated by oxygen atoms of the framework and channel H_2O molecules. Seven additional low-populated Cd sites were located in the channels. Cd-exchanged heulandite was refined in *Cm* symmetry in contrast to most other natural and cation-exchanged heulandites that commonly show *C*2/*m* symmetry. Symmetry lowering is attributed to Si,Al ordering in the tetrahedral framework as well as to the asymmetrical distribution of Cd^{2+} ions due to preferred Cd bonding of oxygen atoms sharing Al-enriched tetrahedra and cation–cation repulsion. © 2000 Elsevier Science B.V. All rights reserved.

Keywords: Cadmium; Crystal structure; Heulandite; Ion exchange; Symmetry lowering; Zeolite

1. Introduction

The toxicological effect of cadmium on the environment is well known. Potential sources of cadmium in wastewater include electroplating, ceramic, alloying, textile and chemical industries and also mine drainage waters. The most common methods of cadmium wastewater treatment are precipitation as hydroxide or sulfide, and ion exchange. However, Cd hydroxide precipitation occurs most effectively at alkaline pH, and ion-exchange resins are unsuitable for mixed cadmium–cyanide solutions [1]. Natural zeolites may be an alternative for wastewater treatment because of their widespread occurrence and low costs. Several studies investigated cadmium removal from solution by various natural zeolites: Blanchard et al. [2] studied the capability of Na-exchanged clinoptilolite to remove Cd^{2+} and other heavy metal ions from drinking water in the presence of ammonium ions. Loizidou and Townsend [3] state that clinoptilolite-Na is superior to clinoptilolite-NH_4 and is more suitable than ferrierite and mordenite to remove cadmium from

* Corresponding author. Fax: +41-31-631-3996.
E-mail address: thomas.armbruster@krist.unibe.ch (T. Armbruster)

PII: S1387-1811(99)00269-3

an effluent. A kinetic study by Assenov et al. [4] yielded the affinity sequence of $Pb^{2+} > Cd^{2+} > Zn^{2+} > Cu^{2+}$ for natural Na-exchanged clinoptilolite. The Cd-exchange kinetics of phillipsite, chabazite [5] and clinoptilolite [6,7] were studied in order to test their usefulness for drinking and wastewater treatment.

Natural zeolites can also be considered for catalytic applications if their chemical and mineral impurities do not affect the catalytic transformations. For example Cd-exchanged clinoptilolite is a very good catalyst for the hydration of acetylene [8,9]. Cd-exchanged zeolites have the advantage that Cd^{2+} remains stable under the respective reaction conditions compared with other transition metal ions in clinoptilolite that are reduced to inactive metals [10].

The previous studies on Cd-exchanged zeolites concentrated on the cation-exchange capabilities, kinetics and catalytic reactivities. However, for further development of applications, it is essential to gain some information about the cadmium distribution within the zeolite cavities and the bonding to the framework structure. Although clinoptilolite that was used in most studies has an excellent cation-exchange capability, the availability of homogeneous, untwinned, mm-size single crystals favors heulandite, which is isostructural to clinoptilolite [11], to perform single-crystal X-ray studies. Clinoptilolite is a variety of heulandite with Si:Al $\geq$ 4.0 [12].

Prior to this study, Stolz and Armbruster [13] produced a partially Cd-exchanged heulandite in 4 M cadmium chloride solution. The acidic exchange solution (pH = 0.35) supplied H_3O^+ and caused partial crystal surface dissolution that provided Al^{3+}, which were both incorporated into the structural channels. Thus, less than two Cd^{2+} per formula unit (pfu) were incorporated. Using a 1 M Cd acetate solution in this study, we succeeded in getting a fully Cd-exchanged heulandite that exhibited *Cm* symmetry in contrast to the structure of partially Cd-exchanged heulandite that was refined in space group *C*2/*m*.

1.1. Heulandite structure and chemistry

Heulandite is a natural zeolite having the simplified formula $(Na,K)Ca_4[Al_9Si_{27}O_{72}] \cdot 24\ H_2O$. The crystal structure (space group *C*2/*m*, $a = 17.70$, $b = 17.94$, $c = 7.42$ Å, and $\beta = 116.40^\circ$, e.g., Refs. [14–18]) exhibits three types of structural channels confined by tetrahedral ring systems. A and B channels are parallel to the *c*-axis (Fig. 1) and are confined by ten- and eight-membered rings of tetrahedra having a highly disordered Si,Al distribution. C channels which are determined by another set of eight-membered rings are parallel to the *a*-axis and the [102] direction [11,19]. Thus, the channel system is two-dimensional parallel to (010).

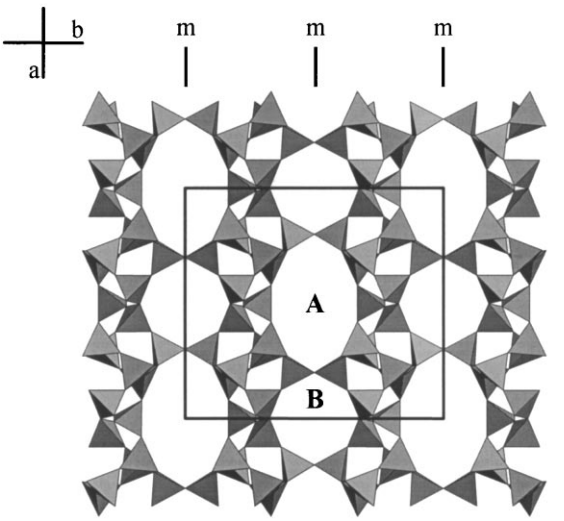

Fig. 1. Tetrahedral model of the heulandite framework projected parallel to the (001) plane, showing the ten-membered A and the eight-membered B channels. Fully Cd-exchanged heulandite exhibits *Cm* symmetry having the mirror plane (m) perpendicular to the *b*-axis.

2. Experimental

Single crystals, about 2–8 mm in diameter, of a natural heulandite $Na_{0.96}K_{0.09}Ca_{3.54}[Al_{8.62}Si_{27.51}O_{72}] \cdot nH_2O$ [20] from Nasik, India [21], were broken to 0.1–0.5 mm fragments, which were placed in a Teflon autoclave filled with 2 M NaCl for 10 weeks and 4 M NaCl for 3 weeks. The NaCl solution was renewed once a week. The exchange reaction was run at 423 K yielding an almost fully Na-exchanged heulandite as a precur-

sor phase. The Na-exchanged heulandite was qualitatively analyzed with a scanning electron microscope (SEM) every 3 weeks during the exchange. Subsequently, Cd^{2+}-exchanged heulandite was obtained by further treatment with a 1 M Cd acetate solution ($Cd(CH_3COO)_2$; pH ≈ 6.0) at 373 K for 64 days. Approximately 200 mg of heulandite-Na was treated in ca. 15 ml of Cd acetate solution once a time and the solution was renewed every 7–10 days. The exchange reaction was quantitatively monitored by measuring the Na^+ ion concentration in the solution.

The composition of the Cd-exchanged heulandite was determined by a CAMECA-SX50 electron microprobe operating at 15 kV and 10 nA beam current with a defocused beam diameter of about 20 μm to minimize sample destruction and the loss of channel cations (measurement time: 20 s on peak; 10 s on background). Albite was used as the standard for Na^+; orthoclase for K^+ and Si^{4+}; anorthite for Ca^{2+} and Al^{3+}; and synthetic Cd_4GeS_6 for Cd^{2+}. Formula calculation was performed on the basis of Al + Si = 36 (Table 1).

The crystal structure of Cd^{2+}-exchanged heulandite was studied by single-crystal X-ray diffraction on an Enraf-Nonius CAD4 diffractometer (graphite-monochromated Mo Kα X-radiation) at 293 K. Data reduction, including background and Lorentz polarization corrections and an empirical absorption correction based on ψ scans, was performed using the SDP [22] program library. The final single-crystal structure refinement using the program SHELX-97 [23] was performed in space group *Cm* with a resultant *R*1 value of 3.35%. A total of 5836 reflections was measured, of which 2283 were unique leading to only eight inconsistent equivalent reflections and an R_{int} value of 1.95%. In addition, merohedral twinning by the pseudo-center of symmetry had to be considered in the acentric *Cm* model, which was in SHELX-97 analyzed by the Flack *x* parameter [24]. The same parameter also indicates whether the absolute structure is correct or whether the structure must be inverted. The Flack *x* parameter exhibited a correct structure set-up and indicated no merohedral twinning. Experimental details of data collection and structure refinement are summarized in Table 1.

Table 1
Data collection and refinement parameters for completely Cd-exchanged heulandite[a]

crystal size (mm)	$0.075 \times 0.150 \times 0.225$
refined composition	$Cd_{4.11}[(Al,Si)_{36}O_{72}] \cdot 30H_2O$
composition by electron microprobe (average of 54 analyses on eight grains)	$Cd_{4.00}Na_{0.01}K_{<0.01}Ca_{0.09}[Al_{8.70}Si_{27.30}O_{71.75}] \cdot nH_2O$
space group	*Cm*
a (Å)	17.714 (4)
b (Å)	17.980(9)
c (Å)	7.417 (2)
β (°)	116.25 (2)
θ max. (°)	30
hkl (min., max.)	$-20 \le h \le 24$, $-25 \le k \le 21$, $-10 \le l \le 9$
scan type	$2.8^\circ\omega + 0.35 \tan\theta$
measured reflections	5836
observed reflections (I > 2 σ(I))	3428
unique reflections	2283
number of parameters	384
R_{int} (%)	1.95
*R*1 (%)	3.35
*wR*2 (%)	8.37
GooF	1.038

[a] Note: $R1 = (\Sigma||F_o| - |F_c||)/(\Sigma|F_o|)$; $wR2 = \{[\Sigma(F_o^2 - F_c^2)^2]/[\Sigma w(F_o^2)^2]\}^{1/2}$; $\text{GooF} = \{[\Sigma w(F_o^2 - F_c^2)^2]/(n-p)\}^{1/2}$.

Moreover, four additional test refinements with the same data set were performed. For refinements in space groups *C*2/*m*, *C*2, and $C\bar{1}$, the lists of the most disagreeable reflections showed the typical characteristics of a wrong space group assignment: F^2_{obs} of mainly weak reflections were larger than F^2_{calc}. Structure refinement in space group *C*1 led to extreme parameter correlations imposed by the pseudo-symmetry of the framework tetrahedra that caused high standard deviation of atomic coordinations and several non-positive definite displacement parameters. These test refinements clearly indicated that the structure of fully Cd-exchanged heulandite is best described in *Cm* diffraction symmetry in contrast to partially Cd-exchanged heulandite (< 2.0 Cd^{2+} pfu) that was refined in space group *C*2/*m* by Stolz and Armbruster [13].

The same nomenclature of channel sites as in the study of Stolz and Armbruster [13] will further be used: the symbol for the chemical element

occupying the site comes first, with the exception of W standing for H_2O molecules. The symbol of the chemical element is followed by A, B, or C, depending on the channel type. A or B alone means that the site is in the center of the channel, whereas A, B, or C followed by a number corresponds to off-centered sites (e.g., Ref. [20]). Atoms related by the pseudo-twofold axes are labeled with a prime notation, e.g., T3 and T3′.

3. Results

The analyzed concentrations of Na^+ ions released to the solution during the Cd exchange of heulandite-Na are given in Table 2. Nine Na^+ pfu correspond to 14.29 mg Na^+ in 200 mg of heulandite-Na assuming an ideal formula of $Na_9[Al_9Si_{27}O_{72}]\cdot 24H_2O$. Since approximately 200 mg of heulandite-Na were treated with Cd acetate solution and a total of 14.76 mg Na^+ were found in solution, cadmium completely replaced sodium in heulandite. The originally colorless–white heulandite crystals adopted a yellowish hue after Cd exchange.

Electron microprobe (EMP) analyses of the Na-exchanged precursor phase gave an average composition of $Na_{8.44}K_{0.01}Ca_{0.09}[Al_{8.63}Si_{27.37}O_{72}]\cdot nH_2O$ with Al varying between 8.26 and 8.96 pfu. This variation conforms with the composition of the natural starting material for which values between $Na_{0.81}K_{0.12}Ca_{3.46}[Al_{8.26}Si_{27.74}O_{71.80}]\cdot nH_2O$ and $Na_{1.07}K_{0.13}Ca_{3.61}[Al_{8.96}Si_{27.04}O_{71.72}]\cdot nH_2O$ were found.

EMP analyses of Cd-exchanged heulandite gave an average composition of $Cd_{4.00}Na_{0.01}K_{<0.01}Ca_{0.09}[Al_{8.70}Si_{27.30}O_{71.75}]\cdot nH_2O$ (normalized to Si + Al = 36). This is in good agreement with the 4.11 Cd^{2+} pfu that were refined from the X-ray data. Fully Cd^{2+}-exchanged heulandite would have the theoretical composition $Cd_{4.5-x}[Al_{9-2x}Si_{27+2x}O_{72}]\cdot nH_2O$ ($x<0.35$). However, traces of Ca, K, and Na were still detected by EMP in the center of some fragments, either because of their larger size or because of structural defects that blocked the free aperture of the channels. The good agreement between the measured composition and the theoretical ratio Cd/Al = 1/2, as well as the only slightly acidic pH of the exchange solution suggested that framework dealumination and H_3O^+ incorporation had not to be considered in contrast to Stolz and Armbruster [13]. Moreover, the average T—O distances of Cd-exchanged heulandite remained within one standard deviation of the Na-exchanged precursor phase [20]. Partially Cd-exchanged heulandite [13] exhibited shorter T—O distances due to partial dealumination of the framework (Table 3).

Table 2
Na^+ accumulation in Cd acetate solution during Cd exchange of heulandite-Na

Days of exchange	20	27	43	60
Na^+ in solution (mg)	13.50	0.85	0.26	0.15
Accumulated amount of exchanged Na^+ (mg)	13.50	14.35	14.61	14.76

The distribution of Cd and H_2O molecules in the A, B, and C channels is shown in Fig. 2. The sites A, A2, B1, and C3 correspond to the sites M(4), M(1), M(2), and M(3) of Koyama and Takéuchi [19]. Atomic coordinates are given in Table 4.

4. Discussion

4.1. Cd and H_2O sites in Cd-exchanged heulandite

Cadmium (ionic radius 0.95 Å) preferentially occupies the center of the A channel (CdA), where it forms a distorted octahedral $Cd^{2+}(H_2O)_6$ complex, as also observed for the smaller divalent cations Mg, Mn, and Cu [13]. Larger divalent cations, such as Ca^{2+} (1.06 Å) in natural heulandite (e.g., Ref. [14]) or Pb^{2+} (1.23 Å) and Sr^{2+} (1.21 Å) in cation-exchanged heulandites [13,26], and Ba^{2+} (1.38 Å) in exchanged clinoptilolite [27], bond to oxygen atoms of the framework and channel H_2O, but never form a hydrous complex in the center of the A channel. All ionic radii cited above are those of Shannon [28] for sevenfold coordination.

Compared with partially Cd-exchanged heulandite [13], completely Cd-exchanged heulandite exhibited six additional low-populated Cd sites,

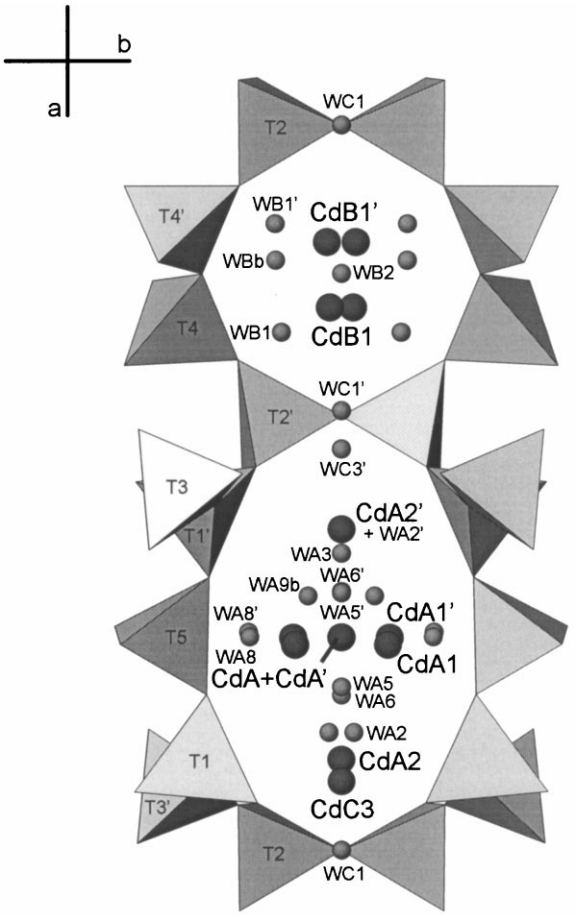

Fig. 2. Distribution of Cd and H_2O sites in the A, B, and C channels of completely Cd-exchanged heulandite. Cd = cadmium and W = H_2O molecule, followed by A, B, or C depending on the channel type. Note that CdB1 has a much higher population than CdB1′.

five in the A and one in the C channel, beside the central CdA site. CdA (population 48%) bonded to WA2, WA2′, WA5′, 2 × WA8′, and WA9b. Owing to the strong positional disorder, Cd—H_2O bonding distances between 2.09 and 2.37 Å were observed for the distorted octahedral $Cd^{2+}(H_2O)_6$ complex. Six- to sevenfold coordination could be found for the low-populated (5–12%) Cd sites. Although some Cd sites were less than 3 Å apart from one another, mutual repulsion did not have to be considered because of the low populations. Coordination and bond distances of Cd^{2+} are given in Table 5.

The B channel contains two cadmium sites (CdB1, population 44% and CdB1′, population 5%), each disordered around the mirror plane yielding two symmetry equivalent positions 0.5 Å apart. Both Cd sites (CdB1 and CdB1′) are sevenfold coordinated by two framework oxygen atoms and five oxygen atoms of channel H_2O (Table 5). These Cd sites correspond to the low-populated (16%) CdB1 sites in partially Cd-exchanged *C*2/*m* heulandite [13]. Pb-exchanged heulandite that was also refined in space group *Cm* by Gunter et al. [26] has only one cation site (Pb2) on the mirror plane within the B channel, whereas the hypothetical position (Pb2′) related by a pseudo-center of symmetry remains vacant. The shift of the CdB1 site from the mirror plane and the resulting disorder that was not observed for Pb^{2+} [26] is explained by the smaller size of Cd^{2+} compared with Pb^{2+}. Another difference between Cd^{2+} and Pb^{2+} in the B channel of heulandite is the coordination by H_2O. Pb^{2+} exhibits a very irregular coordination interpreted by a pronounced electron lone-pair effect. H_2O sites corresponding to WB1′, related by a pseudo-twofold axis to WB1, are not occupied in the Pb-exchanged sample but show a high population in Cd-exchanged heulandite (Fig. 3).

An additional cadmium site, CdC3 (population 10%), was found in the C channel in contrast to Stolz and Armbruster [13], where the C channel was completely occupied by H_2O molecules (WC1′ and WC3′). Six oxygen atoms (Table 5) were within reasonable bonding distance to CdC3, while WC1 (1.65 Å) and WA6 (1.94 Å) may only be occupied if CdC3 is empty. Notice that full occupation of WC1 (Table 4) was assumed but low deficiencies (< 10%) of H_2O are difficult to resolve.

4.2. Symmetry lowering

Commonly, heulandite is refined in space group *C*2/*m* (e.g., Ref. [29]). However, the structure of heulandite was also refined in space groups of lower symmetry, e.g., *Cm* by Merkle and Slaughter [11] and *Cm* and *C*2 by Alberti [14]. Merkle and Slaughter [11] have chosen *Cm* symmetry because X-ray intensity statistics seemed to suggest an acentric model. Their Si,Al distribution derived from T—O bond lengths, however, did not show

Table 3
Interatomic bond distances (Å) in tetrahedra of the Si,Al framework. T−O distances corrected for rotational disorder [25] are in parentheses

Cm	Cd-Heu			*C*2/*m*	Cd-Heu[a]	Na-Heu[b]
T1−O3	1.628(6) (1.643)	T1′−O3′	1.624(6) (1.645)	T1−O3	1.616(3) (1.636)	1.629(2) (1.644)
−O4	1.634(6) (1.652)	−O4′	1.622(6) (1.632)	−O4	1.614(3) (1.631)	1.628(2) (1.640)
−O6	1.642(6) (1.662)	−O6′	1.612(5) (1.619)	−O6	1.626(2) (1.639)	1.644(1) (1.651)
−O9	1.628(6) (1.642)	−O9′	1.627(6) (1.644)	−O9	1.614(2) (1.631)	1.634(2) (1.643)
mean	1.633(6) (1.650)	mean	1.621(6) (1.635)	mean	1.618(3) (1.634)	1.634(2) (1.645)
T2−O1	1.631(3) (1.647)	T2′−O1′	1.665(3) (1.672)	T2−O1	1.629(1) (1.645)	1.642(1) (1.654)
−O2	1.661(6) (1.678)	−O2′	1.653(5) (1.664)	−O2	1.638(3) (1.656)	1.664(1) (1.674)
−O4	1.658(6) (1.673)	−O4′	1.659(6) (1.672)	−O4	1.649(3) (1.666)	1.670(1) (1.680)
−O10′	1.643(6) (1.668)	−O10	1.684(5) (1.690)	−O10	1.644(3) (1.664)	1.665(1) (1.676)
mean	1.648(5) (1.667)	mean	1.665(5) (1.675)	mean	1.640(3) (1.658)	1.660(1) (1.671)
T3−O2′	1.633(6) (1.642)	T3′−O2	1.592(7) (1.612)	T3−O2	1.629(3) (1.645)	1.632(2) (1.643)
−O3′	1.638(6) (1.658)	−O3	1.614(6) (1.632)	−O3	1.641(3) (1.660)	1.633(2) (1.649)
−O7	1.647(6) (1.665)	−O7′	1.600(6) (1.633)	−O7	1.626(3) (1.655)	1.622(2) (1.644)
−O9	1.638(6) (1.652)	−O9′	1.590(6) (1.608)	−O9	1.625(3) (1.641)	1.635(2) (1.644)
mean	1.639(6) (1.654)	mean	1.599(6) (1.621)	mean	1.630(3) (1.650)	1.631(2) (1.645)
T4−O5	1.672(6) (1.686)	T4′−O5	1.584(6) (1.599)	T4−O5	1.616(2) (1.635)	1.630(1) (1.645)
−O7′	1.615(7) (1.645)	−O7	1.607(6) (1.626)	−O7	1.602(3) (1.632)	1.610(2) (1.632)
−O8	1.624(6) (1.642)	−O8′	1.615(6) (1.637)	−O8	1.611(3) (1.629)	1.627(2) (1.641)
−O10	1.640(6) (1.648)	−O10′	1.604(6) (1.630)	−O10	1.608(3) (1.633)	1.627(2) (1.637)
mean	1.638(6) (1.655)	mean	1.603(6) (1.623)	mean	1.609(3) (1.632)	1.624(2) (1.639)
T5−O6	1.638(6) (1.655)	T5−O6′	1.656(5) (1.664)	T5−O6	1.625(3) (1.638)	1.629(1) (1.636)
−O8	1.638(6) (1.654)	−O8′	1.620(7) (1.642)	−O8	1.609(3) (1.630)	1.618(2) (1.633)
mean	1.638(6) (1.655)	mean	1.638(6) (1.653)	mean	1.617(3) (1.634)	1.624(2) (1.635)

[a] Stolz and Armbruster [13]: partially Cd-exchanged heulandite at 293 K.

[b] Yang and Armbruster [20]: Na-exchanged heulandite at 100 K.

significant deviation from *C*2/*m* symmetry. Alberti [14] tested *Cm* and *C*2 models mainly because Ventriglia [30] found heulandite to be strongly piezoelectric. According to Alberti [14] Si,Al order deviating from *C*2/*m* symmetry in natural Ca-rich heulandites cannot be resolved in space groups *Cm* or *C*2 due to the strong pseudo-symmetry imposed by the framework topology.

Cation-exchanged heulandite may also show lower symmetry, e.g., *Cm* for heulandite-Pb [26], $C\bar{1}$ for NH_4- [31], Cs- [20] and $C_2H_5NH_3$-exchanged heulandite [32]. There are mainly two reasons responsible for the symmetry lowering: (1) Si,Al ordering in the tetrahedral framework, where channel cations and H_2O molecules also adopt the lower symmetry or (2) preferred orientation of cations and H_2O molecules for steric reasons, e.g., ionic radii or bonding and/or repulsion forces. A combination of (1) and (2) is also possible.

The Cd distribution in fully Cd-exchanged heulandite, in particular in the B channel, shows an arrangement, which conforms with *Cm* symmetry. The sites CdB1 and CdB1′ which are related by a pseudo-twofold axis exhibit similar oxygen coordination but Cd preferentially occupied the CdB1 site (population 44%) compared with CdB1′ (population 5%). These distinct Cd populations are in agreement with the Si,Al distribution in the adjacent tetrahedra. T2′ and T4 tetrahedra adjacent to CdB1 have longer T−O bond lengths and therefore higher Al concentrations than T2 and T4′ adjacent to low-occupied CdB1′. The Cd distribution on CdB1 and CdB1′ also influences the Cd

Table 4
Positional parameters and B_{eq} (Å^2) with standard deviations in parentheses for completely exchanged heulandite-Cd[a]

Atom	Population	*x/a*	*y/b*	*z/c*	B_{eq} (Å^2)
T1		0.8221 (1)	0.8293 (1)	0.9112 (3)	1.24 (3)
T1′		1.17963 (9)	1.1688 (1)	1.1016 (3)	1.26 (4)
T2		0.7167 (1)	0.9111 (1)	0.5132 (3)	1.25 (3)
T2′		1.2846 (1)	1.0899 (1)	1.5010 (3)	1.23 (3)
T3		0.7059 (1)	0.6918 (1)	0.7174 (3)	1.24 (3)
T3′		1.2922 (1)	1.3071 (1)	1.2886 (3)	1.13 (3)
T4		0.9347 (1)	0.7001 (1)	0.5882 (3)	1.23 (3)
T4′		1.0664 (1)	1.3034 (1)	1.4201 (3)	1.26 (3)
T5		1.0031 (1)	0.78101 (6)	1.0091 (4)	1.38 (2)
O1		0.7055 (5)	1	0.465 (1)	2.6 (2)
O1′		1.3051 (5)	1	1.554 (1)	2.1 (1)
O2		0.7683 (3)	0.8736 (4)	0.3955 (9)	3.0 (1)
O2′		1.2265 (3)	1.1211 (3)	1.6083 (8)	2.2 (1)
O3		0.8136 (4)	0.8438 (3)	1.1181 (9)	2.8 (1)
O3′		1.1821 (4)	1.1551 (4)	0.8878 (9)	3.1 (1)
O4		0.7712 (3)	0.8968 (3)	0.7582 (9)	2.8 (1)
O4′		1.2355 (3)	1.1042 (4)	1.2548 (8)	2.4 (1)
O5		1.0004 (4)	0.6702 (2)	0.497 (1)	2.55 (6)
O6		0.9217 (3)	0.8350 (3)	0.959 (1)	3.2 (1)
O6′		1.0837 (3)	1.1616 (3)	1.0687 (8)	1.88 (9)
O7		0.6217 (3)	0.7351 (3)	0.5526 (9)	3.0 (1)
O7′		1.3745 (4)	1.2650 (4)	1.447 (1)	3.8 (1)
O8		0.9913 (3)	0.7303 (3)	0.8150 (9)	2.8 (1)
O8′		1.0166 (4)	1.2763 (4)	1.1895 (8)	3.4 (1)
O9		0.7872 (3)	0.7474 (3)	0.8180 (8)	2.5 (1)
O9′		1.2153 (3)	1.2509 (4)	1.1913 (9)	2.8 (1)
O10		0.8821 (3)	0.6265 (3)	0.5987 (8)	2.17 (9)
O10′		1.1221 (3)	1.3748 (3)	1.428 (1)	3.3 (1)
CdA	0.483 (4)	1.0010 (2)	1	0.5098 (6)	4.21 (4)
CdA′	0.066 (4)	1.0006 (6)	1	0.374 (2)	1.9 (3)*
CdA1	0.054 (4)	0.991 (1)	1.057 (1)	−0.077 (3)	7.9 (7)*
CdA1′	0.048 (3)	1.0003 (7)	1.0592 (7)	0.140 (2)	3.3 (3)*
CdA2	0.099 (8)	0.834 (2)	1	0.328 (4)	8.7 (8)*
CdA2′	0.122 (6)	1.1521 (7)	1	1.630 (2)	3.2 (2)
WA2	0.5	0.871 (1)	0.013 (2)	0.336 (5)	13.2 (13)
WA2′	1.0	1.1438 (9)	1	1.697 (3)	9.6 (7)
WA3	0.56 (4)	1.115 (3)	1	−0.203 (6)	11.84*
WA5	1.0	0.932 (2)	1	−0.174 (5)	18.0 (9)*
WA5′	0.37 (3)	1.063 (4)	1	−0.134 (9)	11.84*
WA6	0.39 (3)	0.920 (3)	1	0.043 (9)	11.84*
WA6′	0.15 (3)	1.064 (6)	1	0.06 (1)	7.90*
WA8	0.78 (4)	1.001 (1)	0.888 (1)	0.563 (3)	14.2 (9)*
WA8′	0.33 (2)	1.008 (1)	0.887 (1)	0.402 (3)	3.5 (5)*
WA9b	0.67 (2)	1.058 (2)	1.041 (1)	0.310 (5)	17.9 (11)*
CdB1	0.442 (2)	0.95405 (8)	0.5143 (1)	0.7792 (2)	3.55 (4)
CdB1′	0.048 (2)	1.0438 (9)	0.518 (1)	1.229 (2)	4.2 (5)*
WBb	0.28 (2)	0.519 (2)	0.920 (1)	−0.002 (4)	4.9 (7)*
WB1	0.85 (4)	0.920 (1)	0.573 (1)	1.028 (2)	14.1 (5)
WB1′	0.72 (2)	0.5697 (8)	0.9192 (7)	0.978 (2)	6.4 (4)*
WB2	1.0	0.5015 (9)	1	0.547 (2)	6.4 (3)
CdC3	0.101 (3)	0.8016 (4)	1	−0.019 (1)	2.4 (2)*
WC3′	0.29 (5)	0.259 (3)	1	−0.013 (6)	4.6 (12)*
WC1	1.0	0.706 (1)	1	−0.032 (3)	9.2 (5)
WC1′	0.78 (7)	0.311 (3)	1	0.064 (6)	14.6 (14)*

[a] Note: starred atoms were refined isotropically. Those without standard deviations were fixed. Anisotropically refined atoms are given in the form of the isotropic equivalent atomic displacement parameter defined as $B_{eq} = (8/3)\pi^2 \Sigma_i [\Sigma_j (U_{ij} a_i^* a_j^* a_i \cdot a_j)]$.

Table 5
Coordination and bond distances (Å) of Cd^{2+} in Cd-exchanged heulandite

CdA−WA2	2.09(2)	CdA1−O6	2.38(2)	CdA2−O1	2.88(2)
CdA−WA2′	2.28(1)	CdA1−O6′	2.42(2)	CdA2−O2	2.70(1) (2×)
CdA−WA5′	2.37(6)	CdA1−WA3	2.93(3)	CdA2−O3	3.15(1) (2×)
CdA−WA8′	2.22(2) (2×)	CdA1−WA6	2.10(4)	CdA2−WA6	3.10(5)
CdA−WA9b	2.26(2)	CdA1−WA8	2.93(3)	CdA2−WC1	2.63(3)
		CdA1−WA9b	2.59(4)		
CdA′−WA2	2.19(1)	CdA1′−O6	2.39(1)	CdA2′−O1′	3.00(1)
CdA′−WA2′	2.61(2)	CdA1′−O6′	2.56(1)	CdA2′−O2′	2.59(1) (2×)
CdA′−WA6	2.23(6)	CdA1′−WA5	2.35(3)	CdA2′−WA5′	2.83(4)
CdA′−WA6′	3.01(8)	CdA1′−WA5′	2.92(4)	CdA2′−WA9b	2.34(3) (2×)
CdA′−WA8	2.45(2) (2×)	CdA1′−WA8′	2.12(2)	CdA2′−WC3′	2.48(4)
		CdA1′−WA9b	2.18(3)		
CdB1−O1′	2.43(1)	CdB1′−O1	2.63(1)	CdC3−O3	2.96(1) (2×)
CdB1−O10	2.45(1)	CdB1′−O10′	2.45(2)	CdC3−O4	2.38(1) (2×)
CdB1−WB1	2.42(2)	CdB1′−WB1	2.27(2)	CdC3−WA2	2.37(3)
CdB1−WB1	2.69(2)	CdB1′−WB1	2.61(2)	CdC3−WA5	3.00(2)
CdB1−WB1′	2.26(1)	CdB1′−WB1′	2.39(2)		
CdB1−WB1′	2.57(1)	CdB1′−WB1′	2.76(2)		
CdB1−WB2	2.24(1)	CdB1′−WB2	2.79(2)		

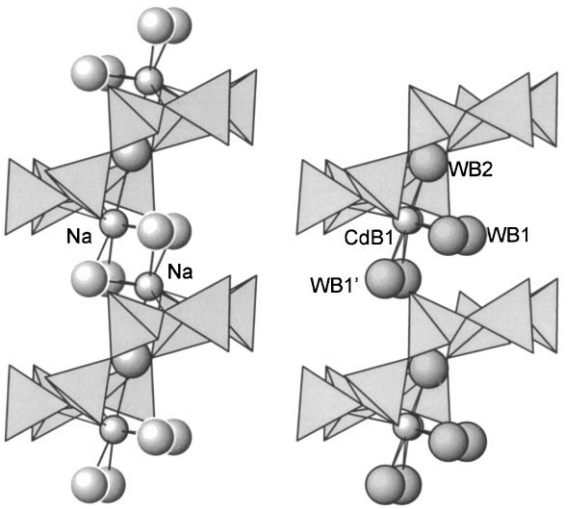

Fig. 3. Cation bonding within the B channel of heulandite with the *c*-axis vertical and the *a*-axis rotated 13° out of the page. Left: arrangement of Na in Na-exchanged precursor phase. The symmetry of the corresponding structure is *C*2/*m*. Right: arrangement of Cd on CdB1 in Cd-exchanged heulandite of *Cm* symmetry. Notice that symmetry lowering leads to a Cd distribution where only each second potential Cd site is occupied. The low occupied site CdB1′ (population 5%) is not shown.

occupancy within the C channel. Only CdC3 (population 10%) is partly occupied but not CdC3′ since the cation–cation repulsion between the hypothetical CdC3′ site and the high-populated CdB1 site would have been too strong.

The tetrahedral framework of Cd-exchanged heulandite clearly exhibits *Cm* symmetry. Most of the framework Al is on the T2 and T2′ tetrahedra with the longest T−O distances. T1′, T3′, and T4′ had the lowest Al content, whereas the Si,Al distribution among the other tetrahedral sites was fairly even. As indicated by the T−O distances given in Table 3, the Si,Al distribution in the tetrahedra was ordered inasmuch as T1, T2′, T3, and T4 had a significantly higher Al content than the T1′, T2, T3′, and T4′ tetrahedra which are related by a pseudo-twofold axis. This is in contrast to Pb-exchanged heulandite refined in space group *Cm*, where the tetrahedral framework structure remained pseudo-centric, with no significant differences in the average T−O distances of tetrahedra related by the pseudo-center of symmetry [26]. However, since Pb has a higher scattering factor than Cd, it contributed more to the bulk electron density of the structure, so that T−O distances could not be resolved as accurately as for Cd-exchanged heulandite. In contrast, symmetry lowering in the Cd-exchanged heulandite was also reflected by the Si,Al ordering in the tetrahedral framework and was not solely induced by the

Cm arrangement of the channel occupants. A correction for tetrahedral rotation according to the riding model of Johnson [25] (distances in parentheses in Table 3), had little effect on the overall Si,Al distribution, although the average T—O distances increased by ca. 0.016 Å. The Si,Al distribution and the Cd bonds to framework oxygen atoms also affect the T—O—T bonding angles (Table 6). The heulandite framework exhibits a considerable flexibility. T—O—T bonding angles of two pseudo-twofold axis related oxygen atoms (e.g., O2 and O2′) differ by up to 8° and the T—O—T bonding angles involving O1′, O2, O6, O7, O9′, and O10′ deviate about 5° from the corresponding T—O—T bonding angles in Na-exchanged heulandite of *C*2/*m* symmetry (Table 6).

The X-ray data of partially Cd-exchanged heulandite showed no indication of symmetry lower than *C*2/*m* [13]. The bow tie like pairs of T2 tetrahedra limiting the B channel had the same Al content and cadmium was evenly distributed among the four symmetry related B1 positions. Moreover, cadmium occupied only the energetically favored CdA and CdB1 sites, since only about 2 Cd pfu were incorporated into the channels. Therefore, no cation–cation repulsion occurred that could have affected the *C*2/*m* cadmium distribution.

Si,Al ordering in the tetrahedral framework and arrangement of channel occupants of Cs^+-exchanged [20], partially NH_4^+-exchanged [31] and $C_2H_5NH_3^+$-exchanged heulandite [32] exhibited even only $C\bar{1}$ symmetry. Yang and Armbruster [20] attributed the symmetry lowering of the diffraction data to the asymmetrical arrangement of the Cs^+ ions. Partial Si,Al ordering in the framework alone would not have distinct enough scattering power to reveal the lower symmetry. In partially NH_4^+-exchanged heulandite, NH_4^+ preferred to occupy an energetically favored N1 site that had stronger bonds to the framework than the 2/*m* symmetry related site [31]. This asymmetric NH_4^+ arrangement enhanced the $C\bar{1}$ diffraction symmetry given by the framework Si,Al distribution. At higher exchange rates both N1 sites become occupied leading to monoclinic diffraction symmetry [33]. $C\bar{1}$ diffraction symmetry of $C_2H_5NH_3^+$-exchanged heulandite is attributed to a high degree of Si,Al ordering within the framework. In this case differences of Si and Al scattering power become dominant and the highly disordered pseudo-monoclinic arrangement of $C_2H_5NH_3^+$ molecules has only little bearing on diffraction data [32]. The common subgroup of space groups $C\bar{1}$ and *Cm* is *C*1. Therefore, one can assume that the frameworks of natural heulandite may exhibit *C*1 symmetry [30,34], but the number, scattering

Table 6
T—O—T bonding angles (°) of Cd- and Na-exchanged heulandite[a]

Na-exchanged heulandite					
T2—O1—T2	157.75(19)	T4—O5—T4	145.87(22)	T5—O8—T4	148.66(10)
T3—O2—T2	144.45(12)	T5—O6—T1	134.65(12)	T1—O9—T3	144.86(9)
T1—O3—T3	143.94(15)	T4—O7—T3	163.36(16)	T4—O10—T2	141.38(13)
T1—O4—T2	140.77(12)				
Cd-exchanged heulandite					
T2—O1—T2	157.15(57)	T4—O5—T4	143.72(27)	T5—O8—T4	151.21(29)
T2′—O1′—T2′	152.14(45)			T5—O8′—T4′	151.47(41)
T3′—O2—T2	153.68(39)	T5—O6—T1	139.95(41)	T1—O9—T3	146.98(27)
T3—O2′—T2′	145.69(34)	T5—O6′—T1′	135.80(34)	T1′—O9′—T3′	149.52(31)
T1—O3—T3′	145.60(42)	T4′—O7—T3	157.21(38)	T4—O10—T2′	142.36(34)
T1′—O3′—T3	145.00(47)	T4—O7′—T3′	160.65(44)	T4′—O10′—T2	146.89(42)
T1—O4—T2	138.69(37)				
T1′—O4′—T2′	137.94(39)				

[a] Yang and Armbruster [20]: Na-exchanged heulandite at 100 K.

power, ionic radii, and arrangement of the channel occupants govern the bulk symmetry that is revealed by X-ray diffraction. Since heulandite-Ca is the most common species [12] and Ca^{2+} ions adopt a highly symmetric configuration and strongly contribute to the X-ray scattering power, heulandite is commonly refined in space group $C2/m$.

Acknowledgements

This study was supported by the Swiss 'Nationalfonds'. We are most grateful to R. Maeder (Mineralogisches Institut der Universität Bern) for assistance during the Na-exchange experiments.

References

[1] J.W. Patterson, in: J.W. Patterson (Ed.), Wastewater Treatment Technology, Ann Arbor Science Publishers, Ann Arbor, MI, 1975, pp. 23–31.
[2] G. Blanchard, M. Maunaye, G. Martin, Water Res. 18 (1984) 1501.
[3] M. Loizidou, R.P. Townsend, J. Chem. Soc., Dalton Trans. 1987 (1987) 1911.
[4] A. Assenov, C. Vassilev, M. Kostova, in: D. Kalló, H.S. Sherry (Eds.), Occurrence, Properties, and Utilization of Natural Zeolites, Akademiai Kiado, Budapest, 1988, pp. 471–480.
[5] C. Colella, M. De'Gennaro, A. Langella, M. Pansini, in: D.W. Ming, F.A. Mumpton (Eds.), Natural Zeolites '93: Occurrence, Properties, Use, International Committee on Natural Zeolites, Brockport, NY, 1995, pp. 377–384.
[6] J.C. Torres, G. Rodriguez-Fuentes, in; Natural Zeolites '97: Program and Abstracts, Ischia, Italy (1997) 293.
[7] H. Faghihian, M.G. Marageh, H. Kazemian, Appl. Radiat. Isotop. 50 (1999) 655.
[8] G. Onyestyak, D. Kalló, in: D.W. Ming, F.A. Mumpton (Eds.), Natural Zeolites '93: Occurrence, Properties, Use, International Committee on Natural Zeolites, Brockport, NY, 1995, pp. 437–445.
[9] D. Kalló, G. Onyestyak, in: Natural Zeolites '97: Program and Abstracts, Ischia, Italy (1997) 176.
[10] G. Onyestyak, D. Kalló, in: Natural Zeolites '97: Program and Abstracts, Ischia, Italy (1997) 236.
[11] A.B. Merkle, M. Slaughter, Am. Mineral. 53 (1968) 1120.
[12] D.S. Coombs, A. Alberti, T. Armbruster, G. Artioli, C. Colella, E. Galli, J.D. Grice, F. Liebau, J.A. Mandarino, H. Minato, E.H. Nickel, E. Passaglia, D.R. Peacor, S. Quartieri, R. Rinaldi, M. Ross, R.A. Sheppard, E. Tillmanns, G. Vezzalini, Can. Mineral. 35 (1997) 1571.
[13] J. Stolz, T. Armbruster, in: C. Colella, F.A. Mumpton (Eds.), Natural Zeolites '97: Occurrence, Properties, Use, Ischia, Italy, International Committee on Natural Zeolites, 2000, in press.
[14] A. Alberti, Tschermaks Mineral. Petrogr. Mitt. 18 (1972) 129.
[15] N. Bresciani-Pahor, M. Calligaris, G. Nardin, L. Randaccio, E. Russo, P. Comin-Chiaromonti, J. Chem. Soc., Dalton Trans. 1980 (1980) 1511.
[16] A. Alberti, G. Vezzalini, Tschermaks Mineral. Petrogr. Mitt. 31 (1983) 259.
[17] T.W. Hambley, J.C. Taylor, J. Solid State Chem. 54 (1984) 1.
[18] T. Armbruster, M.E. Gunter, Am. Mineral. 76 (1991) 1872.
[19] K. Koyama, Y. Takéuchi, Z. Kristallogr. 145 (1977) 216.
[20] P. Yang, T. Armbruster, J. Solid State Chem. 123 (1996) 140.
[21] R.N. Sukheswala, R.K. Avasia, M. Gangopadhay, Mineral. Mag. 39 (1974) 658.
[22] Enraf-Nonius, Structure determination package (SDP), Enraf-Nonius, Delft, The Netherlands, 1983. (computer program).
[23] G.M. Sheldrick, SHELX-97, University of Göttingen, Germany, 1997. (computer program).
[24] H.D. Flack, Acta Crystallogr., Sect A 39 (1983) 876.
[25] C.K. Johnson, in: F.R. Ahmed (Ed.), Crystallographic Computing, Munksgaard, Copenhagen, 1994, pp. 220–226.
[26] M.A. Gunter, T. Armbruster, T. Kohler, C.R. Knowles, Am. Mineral. 79 (1994) 675.
[27] O.E. Petrov, L.D. Filizova, G.N. Kirov, C. R. Acad. Bulg. Sci. 38 (1985) 603.
[28] R.D. Shannon, Acta Crystallogr., Sect A 32 (1976) 751.
[29] G. Gottardi, D. Galli, in: Natural Zeolites, Springer, Berlin, 1985, p. 409.
[30] U. Ventriglia, Rend. Soc. Min. Ital. 9 (1953) 268.
[31] A. Sani, G. Vezzalini, P. Ciambelli, M.T. Rapacciuolo, Microporous Mesoporous Mater. 31 (1999) 263.
[32] J. Stolz, Ph.D Thesis, University of Berne, Switzerland, 1999, p. 184
[33] P. Yang, T. Armbruster, Eur. J. Mineral. 10 (1998) 461.
[34] U. Ventriglia, Periodico Min. 24 (1955) 49.